

# Evidence for a narrow dip structure at 1.9 GeV/c<sup>2</sup> in $3\pi^+3\pi^-$ diffractive photoproduction

E687 Collaboration

P.L. Frabetti<sup>a</sup>, H.W.K. Cheung<sup>b,1</sup>, J.P. Cumalat<sup>b</sup>, C. Dallapiccola<sup>b,2</sup>,  
J.F. Ginkel<sup>b</sup>, W.E. Johns<sup>b,3</sup>, M.S. Nehring<sup>b,4</sup>, E.W. Vaandering<sup>b,3</sup>,  
J.N. Butler<sup>c</sup>, S. Cihangir<sup>c</sup>, I. Gaines<sup>c</sup>, P.H. Garbincius<sup>c</sup>, L. Garren<sup>c</sup>,  
S.A. Gourlay<sup>c,5</sup>, D.J. Harding<sup>c</sup>, P. Kasper<sup>c</sup>, A. Kreymer<sup>c</sup>, P. Lebrun<sup>c</sup>,  
S. Shukla<sup>c,6</sup>, M. Vittone<sup>c</sup>, R. Baldini-Ferrolì<sup>d</sup>, S. Bianco<sup>d</sup>, F.L. Fabbri<sup>d</sup>,  
S. Sarwar<sup>d</sup>, A. Zallo<sup>d</sup>, C. Cawfield<sup>e</sup>, R. Culbertson<sup>e,7</sup>, R.W. Gardner<sup>e,8</sup>,  
E. Gottschalk<sup>e,1</sup>, R. Greene<sup>e,9</sup>, K. Park<sup>e</sup>, A. Rahimi<sup>e</sup>, J. Wiss<sup>e</sup>,  
G. Alimonti<sup>f</sup>, G. Bellini<sup>f</sup>, M. Boschini<sup>f</sup>, D. Brambilla<sup>f</sup>, B. Caccianiga<sup>f</sup>,  
L. Cinquini<sup>f,10</sup>, M. DiCorato<sup>f</sup>, P. Dini<sup>f</sup>, M. Giammarchi<sup>f</sup>, P. Inzani<sup>f</sup>,  
F. Leveraro<sup>f</sup>, S. Malvezzi<sup>f</sup>, D. Menasce<sup>f</sup>, E. Meroni<sup>f</sup>, L. Milazzo<sup>f</sup>,  
L. Moroni<sup>f</sup>, D. Pedrini<sup>f</sup>, L. Perasso<sup>f</sup>, F. Prelz<sup>f</sup>, A. Sala<sup>f</sup>, S. Sala<sup>f</sup>,  
D. Torretta<sup>f,1</sup>, D. Buchholz<sup>g</sup>, D. Claes<sup>g,11</sup>, B. Gobbi<sup>g</sup>, B. O'Reilly<sup>g,12</sup>,  
J.M. Bishop<sup>h</sup>, N.M. Cason<sup>h</sup>, C.J. Kennedy<sup>h,13</sup>, G.N. Kim<sup>h,14</sup>, T.F. Lin<sup>h,15</sup>,  
D.L. Pusejlic<sup>h,13</sup>, R.C. Ruchti<sup>h</sup>, W.D. Shephard<sup>h</sup>, J.A. Swiatek<sup>h,16</sup>,  
Z.Y. Wu<sup>h,17</sup>, V. Arena<sup>i</sup>, G. Boca<sup>i</sup>, G. Bonomi<sup>i,18</sup>, C. Castoldi<sup>i</sup>, G. Gianini<sup>i</sup>,  
M. Merlo<sup>i</sup>, S.P. Ratti<sup>i</sup>, C. Riccardi<sup>i</sup>, L. Viola<sup>i</sup>, P. Vitulo<sup>i</sup>,  
A.M. Lopez<sup>j</sup>, L. Mendez<sup>j</sup>, A. Mirles<sup>j</sup>, E. Montiel<sup>j</sup>, D. Olaya<sup>j,12</sup>,  
J.E. Ramirez<sup>j,12</sup>, C. Rivera<sup>j,12</sup>, Y. Zhang<sup>j,19</sup>, J.M. Link<sup>k</sup>, V.S. Paolone<sup>k,20</sup>,  
P.M. Yager<sup>k</sup>, J.R. Wilson<sup>l</sup>, J. Cao<sup>m</sup>, M. Hosack<sup>m</sup>, P.D. Sheldon<sup>m</sup>,  
F. Davenport<sup>n</sup>, K. Cho<sup>o</sup>, K. Danyo<sup>o,21</sup>, T. Handler<sup>o</sup>, B.G. Cheon<sup>p,22</sup>,  
Y.S. Chung<sup>p,23</sup>, J.S. Kang<sup>p</sup>, K.Y. Kim<sup>p,20</sup>, K.B. Lee<sup>p,24</sup>, S.S. Myung<sup>p</sup>

<sup>a</sup> *Dip. di Fisica dell'Università and INFN-Bologna, I-40126 Bologna, Italy.*

<sup>b</sup> *University of Colorado, Boulder, CO 80309, USA.*

<sup>c</sup> *Fermi National Accelerator Laboratory, Batavia, IL 60510, USA.*

<sup>d</sup> *Laboratori Nazionali di Frascati dell'INFN, I-00044 Frascati, Italy.*

<sup>e</sup> *University of Illinois at Urbana-Champaign, Urbana, IL 61801, USA.*

<sup>f</sup> *Dip. di Fisica dell'Università and INFN-Milano, 20133 Milan, Italy.*

<sup>g</sup> *Northwestern University, Evanston, IL 60208, USA.*

<sup>h</sup> *University of Notre Dame, Notre Dame, IN 46556, USA.*

<sup>i</sup> *Dip. di Fisica Nucleare e Teorica dell'Università and INFN-Pavia, I-27100 Pavia, Italy.*

<sup>j</sup> *University of Puerto Rico at Mayaguez, PR 00681, Puerto Rico.*

<sup>k</sup> *University of California-Davis, Davis, CA 95616, USA.*

<sup>l</sup> *University of South Carolina, Columbia, SC 29208, USA.*

<sup>m</sup> *Vanderbilt University, Nashville, TN 37235, USA.*

<sup>n</sup> *University of North Carolina-Asheville, Asheville, NC 208804, USA.*

<sup>o</sup> *University of Tennessee, Knoxville, TN 37996, USA.*

<sup>p</sup> *Korea University, Seoul 136-701, South Korea.*

<sup>1</sup> Present address: Fermi National Accelerator Laboratory, Batavia, IL 60510, USA.

<sup>2</sup> Present address: University of Massachusetts, Amherst, MA 01003, USA.

<sup>3</sup> Present address: Vanderbilt University, Nashville, TN 37235, USA.

<sup>4</sup> Present address: Adams State College, Alamosa, CO 81102, USA.

<sup>5</sup> Present address: Lawrence Berkeley National Laboratory, Berkeley, CA 94720, USA.

<sup>6</sup> Present Address: Lucent Technologies, Naperville, IL 60563, USA.

<sup>7</sup> Present address: Enrico Fermi Institute, University of Chicago, Chicago, IL 60637, USA.

<sup>8</sup> Present address: Indiana University, Bloomington, IN 47405, USA.

<sup>9</sup> Present address: Wayne State University, Detroit, MI 48202, USA.

<sup>10</sup> Present address: National Center for Atmospheric Research, Boulder, CO, 80305, USA.

<sup>11</sup> Present address: University of Nebraska, Lincoln, NE 68588-0111, USA.

<sup>12</sup> Present address: University of Colorado, Boulder CO 80309, USA.

<sup>13</sup> Present address: AT&T, West Long Branch, NJ 07765, USA.

<sup>14</sup> Present address: Pohang Accelerator Laboratory, Pohang 790-784, Korea.

<sup>15</sup> Present address: National Taitung Teacher's College, Taitung, Taiwan 950.

<sup>16</sup> Present address: Science Applications International Corporation, McLean, VA 22102, USA.

<sup>17</sup> Present address: Gamma Products Inc. Palos Hills, IL 60465, USA.

<sup>18</sup> Present address: Dip. di Chimica e Fisica per l'Ingegneria e per i Materiali, Università di Brescia and INFN-Pavia, Italy.

<sup>19</sup> Present address: Lucent Technologies, Lisle, IL 60532, USA.

<sup>20</sup> Present address: University of Pittsburgh, Pittsburgh, PA 15260, USA.

<sup>21</sup> Present address: Brookhaven National Laboratory, Upton, NY 11793,

USA.

<sup>22</sup> Present address: KEK, National Laboratory for High Energy Physics, Tsukuba 305, Japan.

<sup>23</sup> Present address: University of Rochester, Rochester, NY 14627, USA.

<sup>23</sup> Present address: Korea Research Institute of Standards and Science, Yusong P.O. Box 102, Taejon 305-600, South Korea.

*PACS* : 13.25.Jx, 13.60.Le, 14.40.Cs

---

## Abstract

A narrow dip structure has been observed at  $1.9 \text{ GeV}/c^2$  in a study of diffractive photoproduction of the  $3\pi^+3\pi^-$  final state performed by the Fermilab experiment E687.

---

## 1. Introduction.

The Fermilab Experiment 687 collaboration has collected a large sample of high-energy photoproduction events, recorded with the E687 spectrometer [1][2] during the 1990/91 fixed-target runs at the Wideband Photon beamline at Fermilab. Although the experiment is focussed on charm physics, a very large sample of diffractively photoproduced light-meson events was also recorded. This paper reports on a study of the diffractive photoproduction of the  $3\pi^+3\pi^-$  final state and the observation of a narrow dip in the mass spectrum at  $1.9 \text{ GeV}/c^2$ .

## 2. E687 spectrometer

In E687, a forward multiparticle spectrometer is used to measure the interactions of high-energy photons on a 4-cm-thick Be target. It is a large-aperture, fixed-target spectrometer with excellent vertexing, particle identification, and reconstruction capabilities for photons and  $\pi^0$ 's. The photon beam is derived from the Bremsstrahlung of secondary electrons of  $\approx 300 \text{ GeV}$  endpoint energy, which were produced by the  $800 \text{ GeV}/c$  Tevatron proton beam. The charged particles emerging from the target are tracked by a system of twelve planes of silicon microstrip detectors arranged in three views. These provide

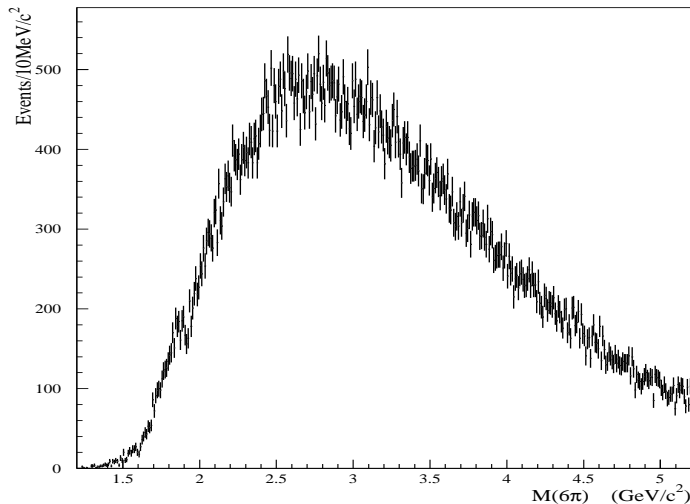


Fig. 1. Distribution of  $3\pi^+3\pi^-$  invariant mass after applying a cut on the total energy deposited in the calorimeters with respect to the total energy in the spectrometer.

high-resolution separation of primary (production) and secondary (charm decay or interaction) vertices. The momentum of a charged particle is determined by measuring its deflections in two analysis magnets of opposite polarity with five stations of multiwire proportional chambers. Three multicell threshold Čerenkov counters are used to discriminate between pions, kaons, and protons. Photons and neutral pions are reconstructed by electromagnetic (EM) calorimetry. Hadron calorimetry and muon detectors provide triggering and additional particle identification.

### 3. Event Selection

Pions are produced in photon interactions in the Be target. The data acquisition trigger requires a minimum energy deposition in the hadron calorimeters located behind the electromagnetic calorimeters and at least three charged tracks outside the pair region. The microstrip system and the forward spectrometer measure the  $6\pi$  final state (in this paper,  $6\pi$  refers to the  $3\pi^+3\pi^-$  state) with a mass resolution  $\sigma = 10 \text{ MeV}/c^2$  at a total invariant mass of about  $2 \text{ GeV}/c^2$ . It is required that a single six-prong vertex be reconstructed in the target region by the microstrip detector, with a good confidence level. Such a requirement rejects background due to secondary interactions in the target. Exclusive final states are selected by also requiring that the same number of tracks be reconstructed in the magnetic spectrometer. The six microstrip tracks and the six spectrometer tracks are required to be linked, with no am-

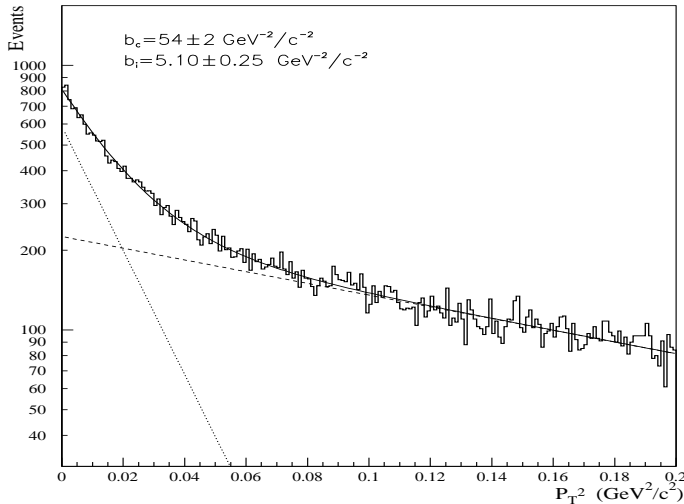


Fig. 2. Transverse momentum squared distribution showing the diffractive peak.

biguity in associating the microstrip and spectrometer tracks. Events with particles identified by the Čerenkov system as definite electrons, kaons, or protons, or as kaon/proton ambiguous are eliminated and at least four out of six particles have to be positively identified as  $\pi^\pm$ . Particle identification is tested by assuming that one or two out of the six tracks is a  $K^\pm$ , by computing all two-track invariant mass combinations, and verifying that there is no evidence of a peak at the  $K^*$  or at the  $\phi$  mass. We eliminated final states with  $\pi^0$ 's by rejecting events with visible energy in the electromagnetic calorimeters that was not associated with the charged tracks. A cut in this variable ( $E_{\text{cal}}/E_{6\pi} \leq 5\%$ ) is applied on the calorimetric neutral energy normalized to the six-pion energy measured in the spectrometer. The distribution of the six-pion invariant mass after these cuts is shown in Fig. 1. The plot shows a structure at  $1.9 \text{ GeV}/c^2$ . In the following, only the  $6\pi$  mass region around this structure will be analyzed.

For diffractive reactions at our energies, the square of the four-momentum transfer  $t$  can be approximated by the square of the total transverse momentum  $P_T^2$  of the diffractively produced hadronic final state. Using this definition, the  $P_T^2$  distribution of diffractive events, Fig. 2, is well described by two exponentials: a coherent contribution with a slope  $b_c = 54 \pm 2 (\text{GeV}/c)^{-2}$  consistent with the Be form factor [3] and an incoherent contribution with a slope  $b_i = 5.10 \pm 0.25 (\text{GeV}/c)^{-2}$ . Taking only events with  $P_T^2 \leq 0.040 \text{ GeV}^2/c^2$ , we evaluated a contamination of about 50% from nondiffractive events. This incoherent contribution shows no structure in the  $1.2\text{--}3.0 \text{ GeV}/c^2$  mass range, Fig. 3. The diffractive mass distribution was obtained by subtracting this contribution, parametrized by a polynomial fit, and dividing the yield by the detection efficiency.

The detection efficiency was computed by modeling diffractive photoproduction of a mass  $M$ , using the experimentally found slope  $b_c$ , and simulating the decay  $M \rightarrow 6\pi$  according to phase space [4]. There is no threshold or discontinuity for the efficiency, particularly in the region of the dip structure. At  $1.9 \text{ GeV}/c^2$ , the (self-normalized relative) efficiency  $A$  varied as  $dA/A/dM_{6\pi} = 0.15/\text{GeV}/c^2$ . The efficiency and the efficiency-corrected distribution of the six-pion invariant mass for diffractive events, in the mass range  $1.4\text{--}2.4 \text{ GeV}/c^2$ , are shown in Fig. 4. There is no evidence, albeit with large combinatorial backgrounds, for resonance substructure, e.g.,  $\rho^0 \rightarrow \pi^+\pi^-$ , in the  $6\pi$  data below  $M_{6\pi} = 2.0 \text{ GeV}/c^2$ , either at the mass region of the dip or in nearby sidebands. Similarly, the efficiency or acceptance exhibited no threshold, edge, or discontinuity over the entire mass region observed, when the six pion state was simulated as a sequence of decays of intermediate two-body resonances, for example  $a_1^+ + a_1^- \rightarrow (\rho^0\pi^+) + (\rho^0\pi^-) \rightarrow (\pi^+\pi^-\pi^+) + (\pi^+\pi^-\pi^-)$ , even under extreme assumptions of full longitudinal or transverse polarizations for the initial state.

The presence of a dip at  $1.9 \text{ GeV}/c^2$  was verified by several checks of the systematics. Diffractive photoproduction of  $D^0\bar{D}^0$  pairs or the associated production of  $\bar{D}^0$  plus a charm baryon at low  $t$  (where the decay products of the other charm meson or charm baryon are missed) followed by the  $6\pi$  decay of the  $D^0$  or  $\bar{D}^0$  are estimated by Monte Carlo simulation to be negligible contributions. It was also checked that demanding more stringent cuts (i.e., requiring that all six particles be identified as  $\pi^\pm$ , applying a sharper cut on the calorimeter neutral energy, or subtracting the incoherent contribution bin by bin) increases the statistical errors without significantly affecting the behavior shown in Fig. 3.

A three-parameter polynomial fit was performed, solid line in Fig. 4, to explore the hypothesis that any structure in this distribution is a statistical fluctuation. The normalized residual distribution, evaluated for each  $10\text{-MeV}/c^2$  bin, is good in the full invariant mass range (Fig. 5: left), with the exception of the interval centered at  $1.9 \text{ GeV}/c^2$ , the region of the claimed dip, where a poor  $\sim 10^{-3}$  confidence level interval (Fig. 5: right), is obtained, making it highly unlikely that the observed dip is a statistical fluctuation. Incoherently adding a Breit-Wigner to the fit does not improve the fit quality much, dashed lines in Fig. 4 and Fig. 5.

#### 4. Fitting the six-pion invariant mass distribution

Because of the narrow width, the E687 spectrometer mass resolution,  $\sigma = 10 \text{ MeV}/c^2$  at  $2 \text{ GeV}/c^2$ , was unfolded by applying the method described in

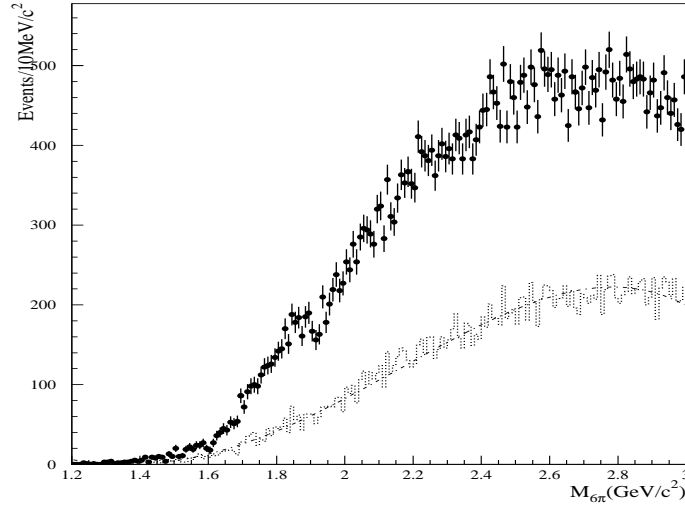


Fig. 3. Distribution of  $3\pi^+3\pi^-$  invariant mass in the 1.2–3.0  $\text{GeV}/c^2$  mass range: coherent plus incoherent contribution. Dotted distribution: incoherent contribution.

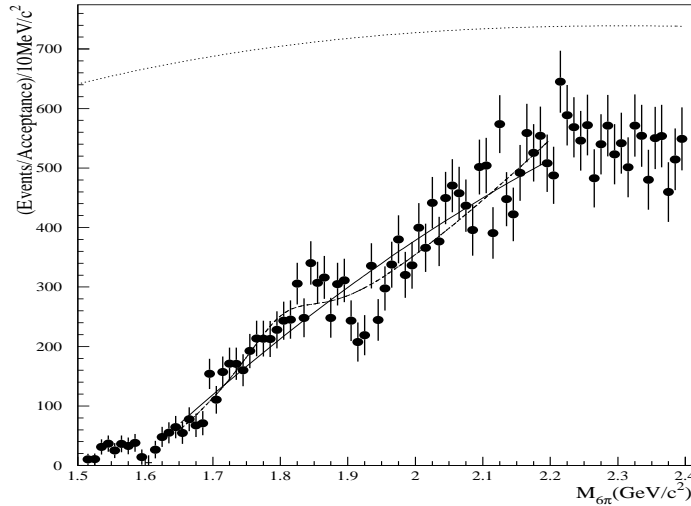


Fig. 4. Acceptance-corrected distribution of  $3\pi^+3\pi^-$  invariant mass for diffractive events after subtracting incoherent contribution. Solid line: second-order polynomial fit. Dashed line: polynomial fit with incoherently-added Breit-Wigner. Upper dot line: relative detection efficiency (arbitrary normalization).

Ref. [5]: the experimentally observed data distribution  $r(x)$  and the unfolded mass distribution  $a(x)$  are related by  $a(x) \sim r(x) - 0.5\sigma^2 \cdot r(x)''$ , where  $r(x)''$  is the second derivative with respect to  $M_{6\pi}$  for the observed distribution. This relationship results from applying a Fourier transform and approximating the resolution function by  $g(x) = \exp(-\frac{\sqrt{2}|x|}{\sigma})$ , which is marginally different from a Gaussian. A fit similar to the following one is used to obtain  $r(x)''$  from the

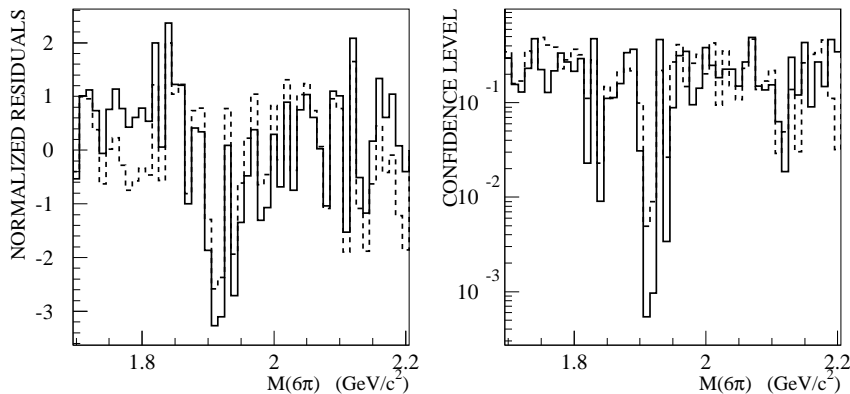


Fig. 5. Normalized residual (left) and confidence level (right) distributions. Solid line: second-order polynomial fit. Dashed line: Breit-Wigner plus second-order polynomial fit.

unfolded data. The data after unfolding are shown in Fig. 6.

The dip structure at  $1.9 \text{ GeV}/c^2$  has been characterized by a two-component fit, adding coherently a relativistic Breit-Wigner resonance to a diffractive continuum contribution. The continuum probability distribution  $F_{JS}(M)$  has been modeled after a Jacob-Slansky diffractive parameterization[6], plus a constant term  $c_0$

$$F_{JS}(M) = f_{JS}^2(M) = c_0 + c_1 \frac{e^{-\frac{\beta}{M-M_0}}}{(M - M_0)^{2-\alpha}}$$

The Jacob-Slansky model is based on probabilities, rather than amplitude phenomenology, and specifically has no prescription as to how the complex phase of the continuum distribution varies with mass. The Jacob-Slansky amplitude  $f_{JS}(M)$  is assumed to be the purely real ( $\phi_{JS} \equiv 0$ ) square root of the probability function  $F_{JS}(M)$ . For the fit, a relative phase factor  $e^{i\phi}$ , independent of mass, and a normalizing factor  $a_r$  multiplied a relativistic Breit-Wigner resonance term, giving the overall amplitude

$$A(M) = f_{JS}(M) + a_r \frac{-M_r \Gamma e^{i\phi}}{M^2 - M_r^2 + iM_r \Gamma}$$

Fit results are shown in Table 1 and in Fig. 6 for a fitted mass range from  $1.65$  to  $2.15 \text{ GeV}/c^2$ , symmetric with respect to the dip. Quantities shown are the mass and width of the resonance, the amplitude ratio  $a_r/f_{JS}(M_r)$  between the Breit-Wigner function and the Jacob-Slansky continuum, the relative phase and the  $\chi^2/\text{dof}$ . The Jacob-Slansky parameters for that one mass range are also given. Fit values show consistent evidence for a narrow



Table 1

Fit results for a mass range from 1.65 to 2.15  $GeV/c^2$ 

$M_r$ ( $GeV/c^2$ )	$1.911 \pm 0.004$
$\Gamma$ ( $MeV/c^2$ )	$29 \pm 11$
$a_r/f_{JS}(M_r)$	$0.31 \pm 0.07$
$\phi$ (deg.)	$62 \pm 12$
$\chi^2/dof$	1.1
$M_0$ ( $GeV/c^2$ )	$1.49 \pm 0.02$
$c_0$ ( $GeV/c^2$ ) <sup>-1</sup>	$0 \pm 50$
$c_1$ ( $GeV/c^2$ ) <sup>1-<math>\alpha</math></sup>	$960 \pm 80$
$\beta$ ( $GeV/c^2$ )	$0.5 \pm 0.3$
$\alpha$	$1.8 \pm 0.2$

resonance at  $M_r = 1.911 \pm 0.004 \pm 0.001$   $GeV/c^2$  with a width  $\Gamma = 29 \pm 11 \pm 4$   $MeV/c^2$ , where the errors quoted are statistic and systematic, respectively. The fit values shown in Fig. 6 and represented by the parameters of Table 1 are stable with acceptable  $\chi^2/dof$  over varying mass ranges from 1.65 to 2.3  $GeV/c^2$ . We quote as systematic error the sample variance of the fit values due to our choice of fit mass range. The quality of the fit deteriorates somewhat as the upper limit of the fit for this simple model is extended from 2.1 to 3.0  $GeV/c^2$ . However, the only fit parameter that is affected is the width, which varies from  $29 \pm 11$   $MeV/c^2$  to  $40 \pm 20$   $MeV/c^2$ .

The dip structure is reminiscent of what was observed in  $e^+e^-$  annihilation [7] [8]. The mechanism by which a narrow resonance may interfere destructively with a continuum, or a broad resonance, could be similar to the one described in [9], in a different context. Vector  $q\bar{q}$  hybrids are predicted at  $\sim 1.9$   $GeV/c^2$  according to the flux tube model [10] [11]. A hybrid is expected to have a small, but not vanishing,  $e^+e^-$  width and a total width constrained by decay selection rules [12]. Vector glueballs are expected at higher masses, according to the bag model and to lattice calculations[13][14]. Narrow resonances have also been predicted near the  $N\bar{N}$  region, but have never been conclusively found [15][16][17][18][19]. A  $N\bar{N}$  threshold effect might also produce a downward step in the amplitude, followed by a recovery[20][21]. These resonances should also be observed as a step variation in the nucleon time-like form factor[22] [23].

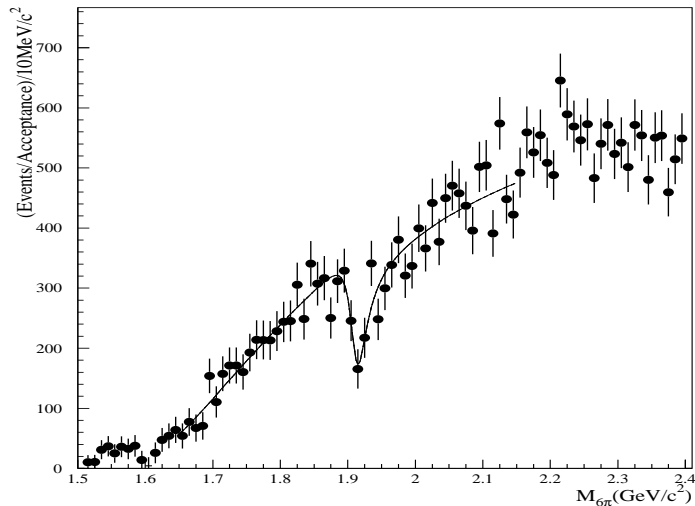


Fig. 6. Acceptance-corrected distribution of  $3\pi^+3\pi^-$  invariant mass for diffractive events. The mass resolution has been unfolded. Fit parameters are listed in Table 1.

## 5. Conclusions

The diffractive photoproduction of  $3\pi^+3\pi^-$  has been studied by E687. Evidence has been found for a narrow structure near  $M_{6\pi} = 1.9 \text{ GeV}/c^2$ . If this dip is characterized as the destructive interference of a resonance with the continuum background, then the parameters of this resonance would be  $M_r = 1.911 \pm 0.004 \pm 0.001 \text{ GeV}/c^2$ , with  $\Gamma = 29 \pm 11 \pm 4 \text{ MeV}/c^2$ . Such a resonance could be assigned the photon quantum numbers ( $J^{PC} = 1^{--}$ ) and  $G=+1, I=1$  due to the final state multiplicity. There is little understanding of the specific mechanism responsible for this destructive interference. In order to facilitate additional phenomenological studies, the data points of Fig. 6 are available [24].

## 6. 2018 Addendum: Comparison of the 6 pion energy distribution with Montecarlo simulation

In September 2018, 17 years after publication, a reader requested the energy distribution of the  $6\pi$  state, which was not included in publication of 2001. This distribution was found in the Fermilab E687/E831 Internal Note six\_pi1.ps, dated 9/15/2000. The figure and descriptive text below as sent to the reader are appended here to provide documentation of this distribution.

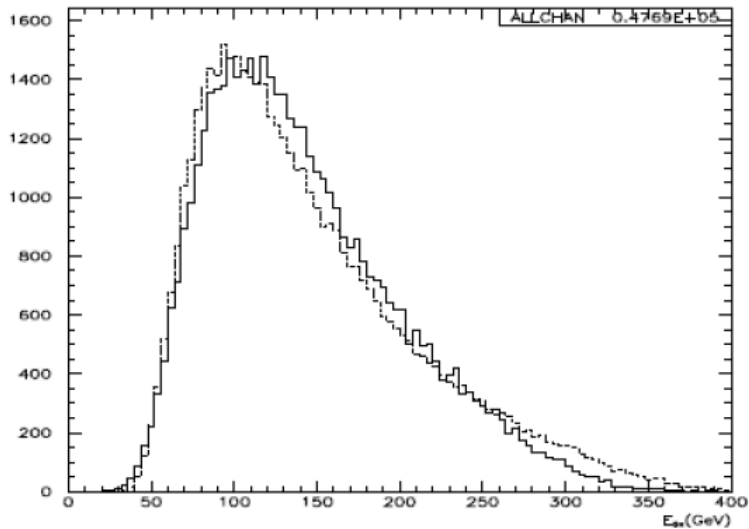


Fig. 7.  $3\pi^+3\pi^-$  energy distribution from E687 data (solid line) and E831 Montecarlo (dashed line).

To simulate E687 data, we have used the E831 Montecarlo with a top energy of 300 GeV. Once generated, the photon energy has been increased by a factor of 350/300 in order to take roughly into account the E687 beam energy. So, our comparison of the energy distribution of our events with the E831 Montecarlo events (Fig. 7) is only approximate.

We would like to thank the staffs of Fermi National Accelerator Laboratory, INFN of Italy, and the physics departments of the collaborating institutions for their assistance. This research was partly supported by the U. S. Department of Energy, the U. S. National Science Foundation, the Italian Istituto Nazionale di Fisica Nucleare and Ministero dell'Università e della Ricerca Scientifica e Tecnologica, the Brazilian Conselho Nacional de Desenvolvimento Científico e Tecnológico, CONACyT-México, the Korean Ministry of Education, and the Korean Science and Engineering Foundation.

1. P.L. Frabetti *et al.* (E687 Coll.), Nucl. Instrum. Meth. A **320**, 519 (1992).
2. P.L. Frabetti *et al.*, Nucl. Instrum. Meth. A **329**, 62 (1993).
3. C.W. De Jager, H. De Vries, and C. De Vries, Atom. Data and Nucl. Data Tables **36** (1987) 495.
4. F. James, GENBOD N-Body Monte-Carlo Event Generator, CERN Computer Centre Program Library.
5. E. Sjøntoft, Nucl. Instrum. Meth. **163** (1979) 519.

6. M. Jacob and R. Slansky, Phys. Lett. B **37** (1971) 408, and Phys. Rev. D **5** (1972) 1847.
7. R. Baldini *et al.*, reported at the "Fenice" Workshop, Frascati(1988).
8. A.B. Clegg and A. Donnachie, Z.Phys. C **45** (1990) 677.
9. P.J. Franzini and F.J. Gilman, Phys.Rev. D **32** (1985) 237.
10. N. Isgur and J. Paton, Phys.Rev. D **31** (1985) 2910.
11. T. Barnes, F.E. Close, and E.S. Swanson, Phys.Rev. D **52** (1995) 5242.
12. P. Page, E.S. Swanson, and A.P. Szczepaniak, Phys. Rev. D **59** (1999) 034016.
13. G.S. Bali *et al.*, UKQCD Collaboration, Phys. Lett. B **309** (1993) 378.
14. C. Morningstar and M. Peardon, Phys. Rev. D **60** (1999) 034509.
15. C.B. Dover, Proc. 4th Int. Symp. on  $N\bar{N}$  Int., Syracuse (1975).
16. I.S. Shapiro, Phys.Rep. **35** (1978) 129.
17. R.L. Jaffe, Phys.Rev. D **17** (1978) 1444.
18. C.B. Dover and J.M. Richard, Ann. Phys. **121** (1979) 70.
19. F. Myhrer and A.W. Thomas, Phys. Lett. B **64** (1976) 59.
20. J. L. Rosner, Phys. Rept. **11** (1974) 189.
21. J. L. Rosner, Phys. Rev. Lett. **21** (1968) 950.
22. G. Bardin *et al.*, Phys. Lett. B **255** (1991) 149.
23. A. Antonelli *et al.*, Nucl. Phys. B **517** (1998) 3.
24. Text file `e687_6pi.txt` in the `src` bundle file for preprint hep-ex/0106029.